Hindawi
Advances in Condensed Matter Physics
Volume 2024, Article ID 5134666, 8 pages
https://doi.org/10.1155/2024/5134666

Research Article

The Optimal Doping Ratio of Fe_2O_3 for Enhancing the Electrochemical Stability of Zeolitic Imidazolate Framework-8 for Energy Storage Devices

Sadem Alsaba,[1] Meshari M. Aljohani,[2] S. A. Al-Ghamdi,[1] Abdulrhman M. Alsharari,[1] M. Sadque,[1] and Taymour A. Hamdalla[1]

[1]*Physics Department, Faculty of Science, University of Tabuk, Tabuk, Saudi Arabia*
[2]*Chemistry Department, Faculty of Science, University of Tabuk, Tabuk, Saudi Arabia*

Correspondence should be addressed to Taymour A. Hamdalla; t-ahmed@ut.edu.sa

Received 29 February 2024; Revised 17 April 2024; Accepted 20 April 2024; Published 7 May 2024

Academic Editor: Tholkappiyan Ramachandran

This paper aims to discover a novel composite material that has great potential for manufacturing high-performance supercapacitors suitable for diverse applications, such as electric vehicles, portable electronics, and stationary energy storage systems. Zeolitic imidazolate framework-8 (ZIF-8) doped by different concentrations up to 5 wt.% of nanosized Fe_2O_3 have been prepared (ZIF-8/Fe_2O_3). The effect of doping ratio 1, 3, and 5 wt.% on the structural and electrochemical properties of ZIF-8/Fe_2O_3 has been investigated. The structural characterization has been carried out using TGA, BET, XRD, and FTIR. The XRD analysis revealed that the crystalline size of our sample increased by approximately 16% as a result of doping ZIF-8 with 5 wt.% of Fe_2O_3. The structural analysis of the doped samples revealed that the material exhibited enhanced thermal stability and porosity, with an increase of approximately 105 m^2/g. The introduction of doped nanometal oxides improved the capacitance value of ZIF-8 by significantly increasing its surface area. Additionally, the electron transport efficiency within ZIF-8/5 wt.% Fe_2O_3/electrode is increased. The Nyquist plot decreases as the doping of Fe_2O_3 increases. This indicates a decrease in the charge transfer resistance at the electrode–electrolyte interface, which is desired in applications such as batteries, fuel cells, or electrochemical sensors where faster electron transfer is needed for improved performance.

1. Introduction

The progress in photovoltaic and energy storage technology largely depends upon the discovery and development of innovative materials with enhanced structural, photoelectric, and electrochemical properties [1, 2]. Specifically, metal–organic frameworks (MOFs) have demonstrated considerable promise, especially zeolitic imidazolate framework-8 (ZIF-8), due to their numerous attractive properties, such as high porosity, chemical stability, and customizable functionalities [3, 4]. The molecular structure of ZIF-8 is shown in Scheme 1. Among these, ZIF-8 has emerged as a promising candidate owing to its unique structure and intriguing material properties. Renowned for its high porosity, chemical stability, and customizable functionalities, ZIF-8 has the potential to revolutionize the capabilities of energy devices. Moreover, when paired with nanosized metal oxide nanoparticles particles, the structural, photoelectric, and electrochemical properties of ZIF-8 are significantly optimized [5]. This enhancement facilitates an even broader range of applications in photovoltaic and energy storage technology.

ZIF-8 can be synthesized at room temperature using an aqueous solution and is known for its exceptional thermal and chemical stabilities [6]. ZIF-8 has diverse applications in multiple catalytic fields, including photocatalysis, due to its high photocatalytic efficiency [7]. It has been shown to efficiently degrade reactive black KN-B dye under UV irradiation [8]. ZIF-8 also has applications in environmental remediation, as it exhibits high photostability and effective reusability [9]. Additionally, it has applications in various fields, including the removal of heavy metals, wastewater treatment, gas separation, drug delivery, heterogeneous catalysis, electrochemical

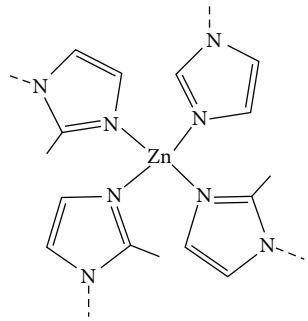

Scheme 1: The molecular structure of ZIF-8.

sensors, and electrode materials for batteries [10]. Furthermore, ZIF-8 can be incorporated into Cu-based precursor solutions to control the phase structure and morphology of composites, leading to enhanced photocatalytic efficiency and cycle stability [8].

Fe_2O_3 is used in different applications such as photocatalytic activity, which arises from its narrow band gap and ability to absorb visible light effectively. Fe_2O_3 nanoparticles possess high electron mobility and good electrochemical activity [11]. These properties can promote charge transport in ZIF-8 and assist in its electrochemical performance, like enhancing charge storage capacity and stability of the material, essential parameters for energy storage devices. Furthermore, Fe_2O_3 nanoparticles exhibit robust chemical stability and can improve the resistance of ZIF-8 to degradation under operational conditions, thereby enhancing the device's longevity. The small size and high surface area of nanosized Fe_2O_3 allow for homogeneous distribution within the material framework, ensuring consistent enhancement of properties throughout the ZIF-8 structure. To assess the efficiency and potential limitations of a specific electrochemical system, various measurements can be conducted. (1) Current–voltage (I–V) curves can aid in determining the system's efficiency, charge/discharge characteristics, and any limitations. (2) Impedance spectroscopy can offer insights into the system's internal resistance, charge transfer resistance, and overall performance. (3) Cyclic voltammetry (CV) can offer information on the system's electrochemical behavior, including its redox processes, capacitive behavior, and kinetic limitations.

Here, the structural and electrochemical properties of different doping ratios of Fe_2O_3 within ZIF-8 have been investigated. This research will improve our understanding and capacity to optimize ZIF-8 for various energy applications. Scheme 2 outlines the experimental procedure used in our manuscript. We are confident that our ZIF-8/Fe_2O_3 could be advantageous in a range of energy applications.

2. Experimental Procedure

2.1. ZIF-8/1, 3, 5 Wt.% Nanosize Fe_2O_3 Samples Fabrication. All the used chemicals have been purchased from Sigma–Aldrich. For preparing an as-prepared sample of ZIF-8, we dissolved 1 g of ZIF-8 in a specified 10 ml of ethanol in a beaker. To ensure complete dissolution, we use a magnetic stirrer. For preparing ZIF-8/1 wt.% Fe_2O_3, 0.99 g of ZIF-8, and 0.01 g of nanosize Fe_2O_3 have been dissolved in 10 ml ethanol, while constantly stirring to avoid the formation of clumps or precipitates. For the preparation of ZIF-8/3 wt.% Fe_2O_3, 0.97 g of ZIF-8 and 0.03 g of nanosized Fe_2O_3 were dissolved in 10 ml of ethanol. Finally, ZIF-8/5 wt.% Fe_2O_3, 0.95 g of ZIF-8, and 0.05 g of nanosize Fe_2O_3 have been dissolved in 10 ml ethanol. After adding all the nanosize Fe_2O_3, we use a sonicator to ensure a homogeneous distribution of ZIF-8 and Fe_2O_3.

2.2. Preparation of ZIF-8/Fe_2O_3 NPs Modified GCE. To examine the electrochemical properties of the ZIF-8/Fe_2O_3, a glassy carbon electrode (GCE) was utilized. The GCE was cleaned by spraying the water and diluted hydrochloric acid over the electrodes and then drying it. ZIF-8/Fe_2O_3 in the colloidal NPs solution was inserted properly in the GCE. The three-electrode system consisted of Pt, GC, and SC (saturated calomel acting as a reference). Within the potential; between −0.4 and 1.4 V, the CV measurement was conducted in KOH (0.1 M) solution as the electrolyte, and at a rate of scanning of about 50 mV/s. The ZIF-8/Fe_2O_3 GCE was dried in an oven for about 3 hr.

2.3. Instrumentation. The XRD for our prepared samples was done using a Shimadzu X-ray diffractometer (CuKα −1.541 Å) with a scan rate of 2°/m and the scans were performed at 2θ angles between 10° and 80°. The XRD model is FRINGE CLASS Benchtop X-ray diffractometer (Lan scientific). The thin film structure was examined using FTIR (Shimadzu Japan, FT-IR 8400S Spectro-photometer using the Kbr pellet method) in the 400–4,000 cm^{-1} spectral region. An electrochemical system (CS-300, 150) was used to measure the electrochemical characteristics. The electrochemical system contains a potentiostat (Model CS350M, Corrtest) to control the potential state and three electrodes—a working electrode, a counter electrode, and a reference electrode. These components work together to accurately measure and control electrochemical reactions within the system.

3. Results and Discussion

3.1. Structural Characterization

3.1.1. XRD. XRD is widely used in investigating the crystallinity of organic materials. Figure 1 shows the XRD spectra for (a) as-prepared (ZIF-8), (b) 1 wt.% Fe_2O_3, (c) 3 wt.% Fe_2O_3, and (d) 5 wt.% Fe_2O_3. As we can see from the figure that the doping ratio of Fe_2O_3 leads to changes in the crystal structure of the ZIF-8 framework. As shown in the figure, the Miller indices of ZIF-8 are (011), (002), (012), and (022) [12]. The Fe_2O_3 diffusion act to increase the intensities of the miller indices related to ZIF-8 such as (011), (002), and (012) at 7.3°, 12.6°, and 14.6°, respectively. The doping of Fe_2O_3 within ZIF-8 introduced XRD peaks associated with the crystal planes of Fe_2O_3 as the peaks around $2\theta° = 33°$, 41°, and 54° which correspond to (012), (113), and (024), respectively [13, 14].

Scherrer's equation was used to evaluate the crystallite size (D) [15]:

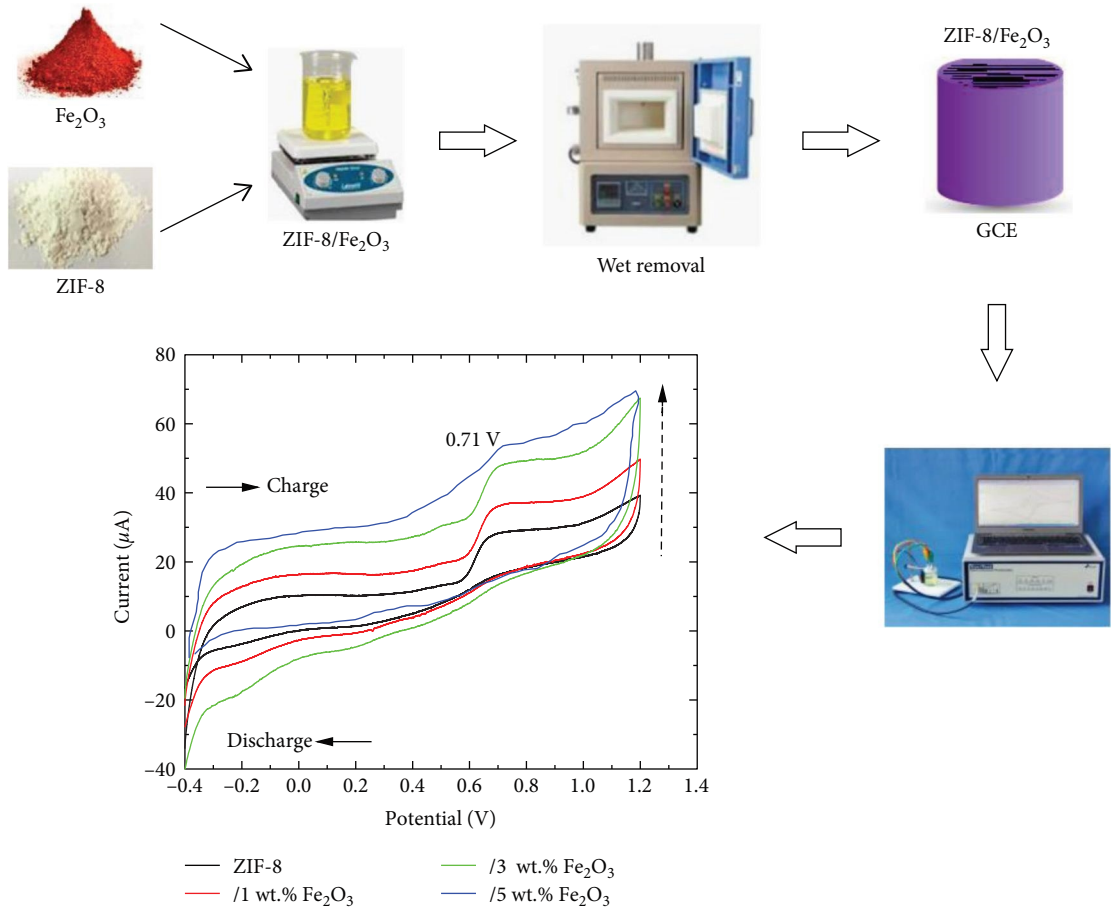

Scheme 2: The experimental procedure for our manuscript.

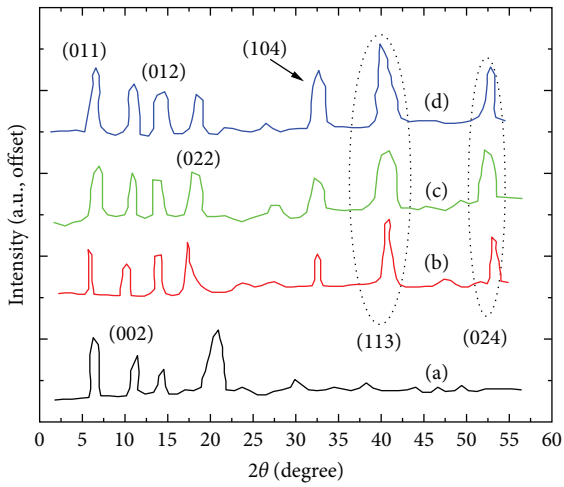

Figure 1: XRD spectra for (a) as-prepared (ZIF-8), (b) 1 wt.% Fe_2O_3, (c) 3 wt.% Fe_2O_3, and (d) 5 wt.% Fe_2O_3.

$$D = \frac{k\lambda}{\eta \cos\theta}, \tag{1}$$

where λ is the X-ray wavelength, K is Scherrer's constant, η is the full width at half maximum, and θ is the Bragg's angle.

The average crystalline size of for (a) as-prepared (ZIF-8), (b) 1 wt.% Fe_2O_3, (c) 3 wt.% Fe_2O_3, and (d) 5 wt.% Fe_2O_3 are 49, 52, 56, and 57 nm. The crystalline size of our sample increased by about 16% due to the doping of Fe_2O_3 by 5 wt.%. This can be beneficial for electrochemical applications where efficient charge transfer is required. The increase in the grain size can lead to electron transport improving within the material, resulting in enhanced electrical conductivity [16]. This can be beneficial for electrochemical applications where efficient charge transfer is required. The dislocation density, the microstrain, and crystallite number are calculated, respectively [17]:

$$\sigma = \frac{1}{D^2}, \tag{2}$$

$$\varepsilon_s = \frac{\eta \cos\theta}{4}, \tag{3}$$

$$N_C = \frac{d}{D^3}. \tag{4}$$

The calculated crystal parameters of ZIf-8/0, 1, 3, and 5 wt.% Fe_2O_3 samples are listed in Table 1.

Table 1: Crystal structural parameters for ZIF-8/0, 1, 3, and 5 wt.% Fe_2O_3.

Sample	XRD parameters		
	δ ($\times 10^{14}$ line/m^2)	ε_s ($\times 10^{-3}$)	N_c ($\times 10^{15}$ m^{-2})
ZIF-8	8.21	1.11	4.51
ZIF-8/1 wt.% Fe_2O_3	7.32	1.05	4.38
ZIF-8/3 wt.% Fe_2O_3	7.01	0.97	4.18
ZIF-8/5 wt.% Fe_2O_3	6.95	0.82	4.01

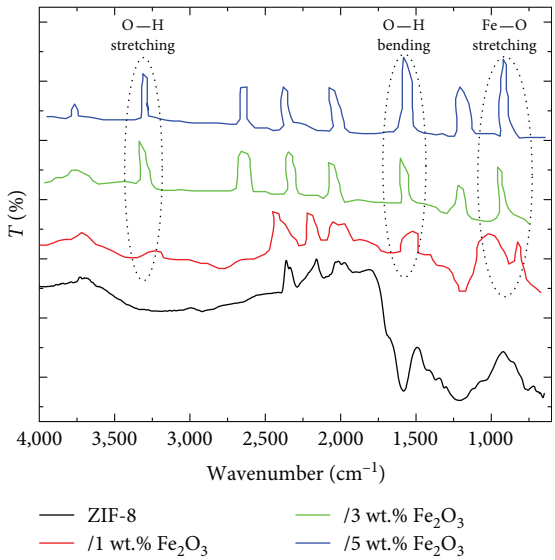

Figure 2: FTIR for pure ZIF-8 and ZIf-8/1, 3, and 5 wt.% Fe_2O_3.

3.1.2. FTIR Analysis. Figure 2 shows the FTIR spectra of ZIf-8/0, 1, 3, and 5 wt.% Fe_2O_3 in the wavenumber region 4,000–400 cm^{-1}. According to the figure, broad and strong absorption bands could appear around 3,430and 1,630 cm^{-1}, which correspond to the O—H stretching vibration and bending vibrations, respectively, due to absorbed water in Fe_2O_3. The peak around 540 cm^{-1} is typically attributed to Fe—O stretching vibration modes in Fe_2O_3. The peak at 1,576 cm^{-1} represents the stretching vibrations of C=N in the imidazole ring. The peak found typically at 758 cm^{-1} portrays the C—H out-of-plane bending mode of the imidazole ring. A peak around 1,150 cm^{-1} represents the C—N stretching vibrations in the imidazole ring. The FTIR peaks correspond with the previously published work [18, 19].

3.1.3. TGA Analysis. Thermal gravimetric analysis (TGA) can potentially be used to examine the weight loss and thermal stability for novel organic composites. Figure 3 shows the TGA analysis for different concentrations (0, 1, 3, and 5 wt.%) of Fe_2O_3 in ZIF-8. The decrease in mass of ZIF-8/Fe_2O_3 NPs was measured at different temperatures up to 780°C. As the temperature reaches 320°C, the mass loss of ZIF-8/0, 1, 3, and 5 wt.% Fe_2O_3 was about 32%, 18%, 14%, and 11%, respectively. This observation assured that Fe_2O_3

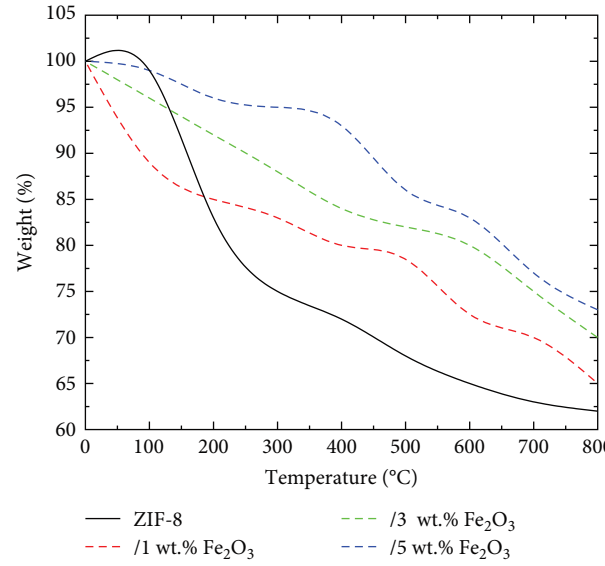

Figure 3: TGA analysis for pure ZIF-8 and ZIf-8/1, 3, and 5 wt.% Fe_2O_3.

NPs improve the thermal resistance and decrease weight loss. And ZIF-8/5 wt.% Fe_2O_3 was the sample with the highest thermal stability. The addition of Fe_2O_3 NPs to ZIF-8 could improve the dispersion of ZIF-8 particles within the composite material. This improved dispersion may result in better thermal conductivity and reduced mass transport during TGA analysis, leading to a decrease in weight loss. The improved thermal stability provided by the addition of Fe_2O_3 NPs to ZIF-8 can be advantageous for energy storage devices [20]. Energy storage systems often involve high temperatures or thermal cycling, and the increased thermal stability can help maintain the structural integrity of the composite material, enhancing its lifespan and performance.

3.1.4. BET Analysis. The analysis of surface area was performed using surface area and pore analyzer from Quantichrome Instruments (Nova 2200e). The BET surface analysis showed a value of 1,048, 1,085, 1,105, and 1,198 m^2/g for ZIF-8/0, 1, 3, and 5 wt.% Fe_2O_3, respectively. The pore diameter of ZIF-8/0, 1, 3, and 5 wt.% Fe_2O_3 was found to be 52.56, 61.43, 65.00, and 67.23 Å, respectively. This could be explained because the addition of nanosized Fe_2O_3 may introduce additional porosity or modify the existing porosity of ZIF-8. Higher porosity provides a larger surface area within the material. Figure 4 shows the BET analysis for ZIf-8/0, 1, 3, and 5 wt.% Fe_2O_3. As we can see from the figure, the increase in the specific area and pore diameter of our samples are 14% and 27%, respectively. This increased surface area allows for more active sites where electrochemical reactions can occur, enhancing the overall energy storage capacity and efficiency [21]. Furthermore, the nanoparticles may also prevent the aggregation of ZIF-8 particles. This helps maintain a larger surface area, which can potentially improve its ability to absorb different substances, including heavy metals and organic pollutants.

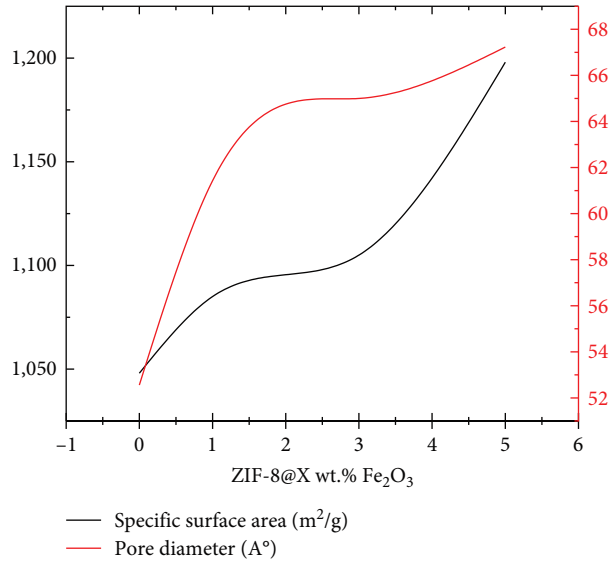

Figure 4: The BET analysis for pure ZIF-8 and ZIf-8/1, 3, and 5 wt.% Fe_2O_3.

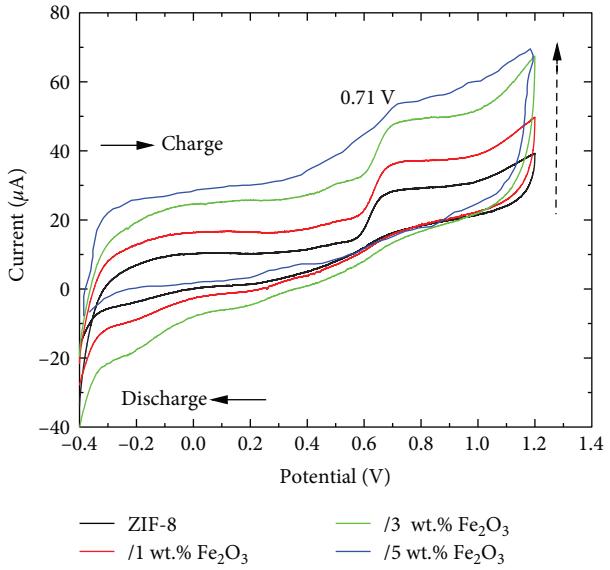

Figure 5: CV curves of ZIf-8/0, 1, 3, and 5 wt.% Fe_2O_3 electrodes at 20–100 mV/s.

3.2. Electrochemical Studies

3.2.1. Cyclic Voltammetry. CV is a widely used electrochemical technique that measures the current response of an electrode material as a function of applied potential. In the case of ZIF-8 doped with nano-Fe_2O_3, CV can provide valuable information about its electrochemical behavior and energy storage capabilities. Figure 5 shows the CV curves of ZIF-8/0, 1, 3, and 5 wt.% Fe_2O_3 electrodes at 20–100 mV/s. Figure 5 displays curves that have a quasirectangular shape. These curves show redox peaks, which indicate the behavior of an electrical double-layer capacitor (EDLC) with fast charging and discharging capabilities of the materials. This indicates a superior capacitance capability that could generate a higher current density.

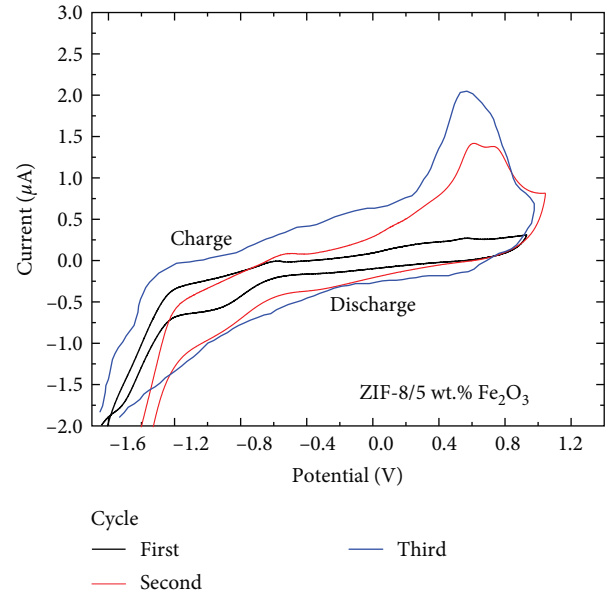

Figure 6: Charge and discharge of ZIf-8/5 wt.% Fe_2O_3 electrodes for three different cycles.

Figure 6 shows the charge and discharge for the highest doped sample (ZIF-8/5 wt.% Fe_2O_3). As we can see, it can be observed that there is a different distribution in this electrode. This is due to its ability to improve the faradic property, which can be seen in the redox peaks of the curve. As a result, this electrode is valuable for creating an exceptional EDLC. The detailed analysis of the intensity and shape of redox peaks in the cyclic voltammogram can indicate the behavior of an EDLC, in which the potential and the current intensity at which the redox peaks occur in the CV results for our investigated material are 1.1 eV and 2 mA [22]. The doped nanometal oxides improve ZIF-8 capacitance value due to the higher electron transport efficiency within ZIF-8/5 wt.% Fe_2O_3/GCE [23]. The uneven distribution observed in the ZIF-8/5 wt.% Fe_2O_3 electrode, as mentioned in Figure 6, is attributed to the unique structure of the composite material. The presence of ZIF-8 and Fe_2O_3 nanoparticles in the electrode creates localized regions with varying concentrations, leading to nonuniform current distribution during charge–discharge cycles. This nonuniformity can enhance the faradic properties of the electrode by promoting heterogeneous reactions at different active sites within the electrode material. This spatial variation in reactivity can facilitate improved utilization of active materials, enhanced electron transport, and overall battery performance.

The current's magnitude in CV measurements, commonly called the peak current, can be determined by utilizing the Randles–Sevcik equation. This equation serves as a mathematical model in the field of electrochemistry of the peak current (i_p) as in the Randles–Sevcik equation [24]:

$$i_p = 2.69 \times 10^5 n^{3/2} A D^{1/2} v^{1/2} c, \quad (5)$$

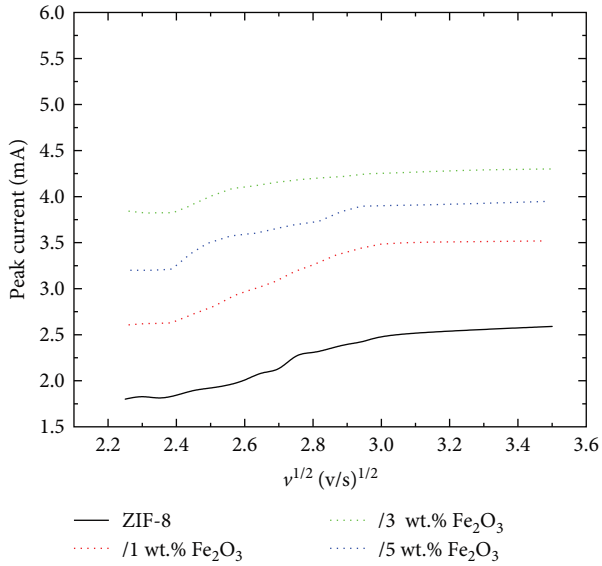

Figure 7: The cathodic peak current (i_p) and ($v^{1/2}$) for ZIf-8/0, 1, 3, and 5 wt.% Fe_2O_3 electrodes.

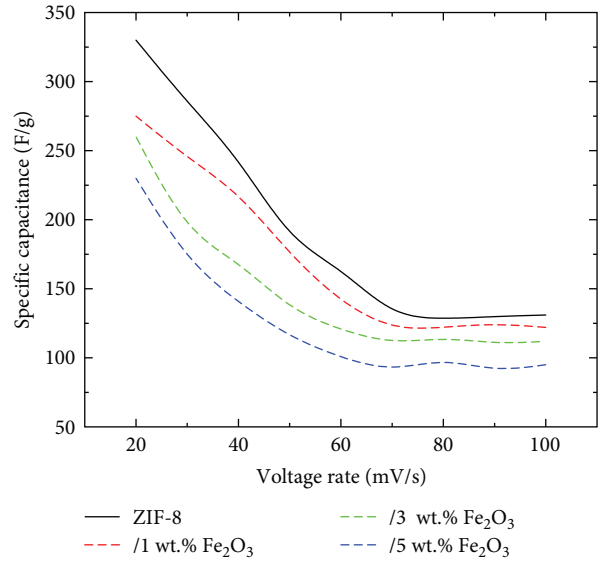

Figure 8: The specific capacitance and scan voltage rate for ZIf-8/0, 1, 3, and 5 wt.% Fe_2O_3 electrodes.

where i_p, n, A, and D are the peak current, electron numbers involved in the redox reaction, the working electrode area (cm^2), and the analyte diffusion coefficient (cm^2/s), respectively. Figure 7 shows the cathodic peak current (i_p) and the square root of the scan rate ($v^{1/2}$) for ZIF-8/0, 1, 3, and 5 wt.% Fe_2O_3 electrodes. Electrode reactions in pure and doped electrodes all show a linear connection between i_p and $v^{1/2}$. Based on our findings, the 5% Fe_2O_3-doped ZIF-8 electrode material exhibited the highest proton transfer coefficient.

3.2.2. Specific Capacitance. The capacitance, C, of our doped MOF can be determined by using the following equation [17]:

$$C = \frac{1}{\mathrm{mv}(V_C - V_a)\int_{V_a}^{V_c} I(V)dV}, \quad (6)$$

where I, V, and m are the applied current applied, the rate of the potential in (mV/s), and m is load mass, respectively. The specific capacitance (F/g) is given by the following equation:

$$C_s = \frac{I\Delta t}{m\Delta V}, \quad (7)$$

where I and m are the discharge current and the weight of deposited material, respectively. Figure 8 depicts the specific capacitance and scan voltage rate for ZIF-8/0, 1, 3, and 5 wt.% Fe_2O_3 electrodes. It is clear from the figure that the capacitance decreases with current density increases for activated pure ZIF-8 and the doped ZIF-8 and this is due to the ions diffusing from the electrolyte toward the electrode material's pores. These curves show redox peaks, which indicate the behavior of an EDLC with fast charging and discharging capabilities of the materials with an average capacitance value of 220 F/g can be considered relatively high and indicative of a good performance, as it suggests a high charge storage capacity per unit mass [25, 26]. Table 2 shows the specific capacitance at different scanning rates for (a) as-prepared (ZIF-8), (b) 1 wt.% Fe_2O_3, (c) 3 wt.% Fe_2O_3, and (d) 5 wt.% Fe_2O_3.

Table 2: The specific capacitance for (a) as-prepared (ZIF-8), (b) 1 wt.% Fe_2O_3, (c) 3 wt.% Fe_2O_3, and (d) 5 wt.% Fe_2O_3.

Sample	Specific capacitance		
	30 mV/s	60 mV/s	90 mV/s
ZIF-8	286	156	125
ZIF-8/1 wt.% Fe_2O_3	233	145	115
ZIf-8/3 wt.% Fe_2O_3	172	121	104
ZIf-8/5 wt.% Fe_2O_3	156	95	92

3.2.3. Impedance Spectroscopy (Nyquist Plot). Nyquist plot is a graphical representation used in electrochemical impedance spectroscopy (EIS) to analyze and interpret the electrical behavior of a system. EIS is important for investigating the electrochemical properties for optimizing performance for energy storage applications. Figure 9 shows the Z′ plotted against Z″ for ZIF-8/0, 1, 3, and 5 wt.% Fe_2O_3 electrodes. It is clear from the figure that bulk resistance decreased by incorporating the nanometal oxide from 1,920 to 1,440 kΩ. The decrease in impedance observed in the Nyquist plot can be due to several factors. For instance, it may indicate a reduction in the charge transfer resistance at the electrode–electrolyte interface, suggesting improved kinetics of the electrochemical reactions. This is often desired in applications such as batteries, fuel cells, or electrochemical sensors where faster electron transfer is desired for enhanced performance.

4. Conclusion

In this paper, we delve into the transformative role of nanosized Fe_2O_3 in augmenting the properties of ZIF-8, thereby

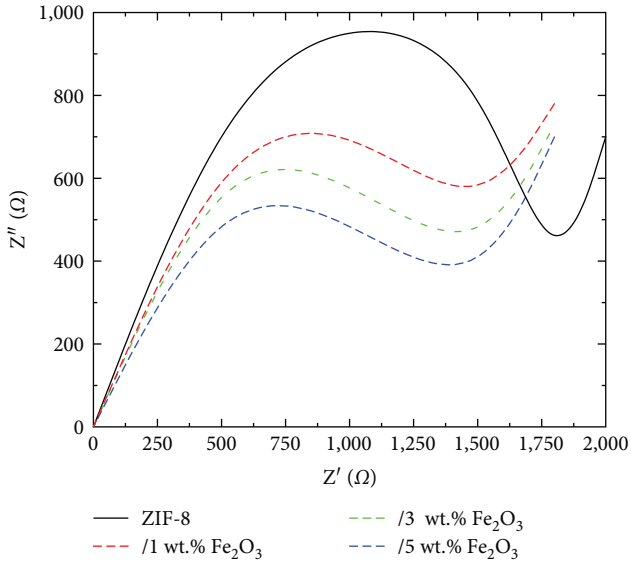

FIGURE 9: Z′ plotted against Z″ for ZIf-8/0, 1, 3, and 5 wt.% Fe_2O_3 electrodes.

charting new courses in the development of highly efficient photovoltaic and energy storage devices. The TGA analysis of our fabricated samples showed that as the temperature reaches 320°, the mass loss of ZIF-8 at 0, 1, 3, and 5 weight percent Fe_2O_3 was about 32%, 18%, 14%, and 11%, respectively, and the increased thermal stability can help to maintain the structural integrity of the composite material, enhancing its lifespan and performance. The BET results confirmed that the porosity of our composite increased when nonmetallic oxides were added, and the addition of 5 wt.% Fe_2O_3 to ZIF-8 resulted in a pore diameter of approximately 67.56 A. The Nyquist plot decreases as the doping of Fe_2O_3 increases. This indicates a decrease in the charge transfer resistance at the electrode–electrolyte interface, which is desired in applications such as batteries, fuel cells, or electrochemical sensors where faster electron transfer is needed for improved performance.

Data Availability

The datasets generated and analyzed during the current study are available from the corresponding author upon reasonable request.

Conflicts of Interest

The authors declare that there are no conflicts of interest in the manuscript.

Acknowledgments

The authors extend their appreciation to the Deanship of Research and Graduate Studies at University of Tabuk for funding this work through Research no. 009-1444-S.

References

[1] E. Pomerantseva, F. Bonaccorso, X. Feng, Y. Cui, and Y. Gogotsi, "Energy storage: the future enabled by nanomaterials," *Science*, vol. 366, no. 6468, Article ID eaan8285, 2019.

[2] C. Liu, F. Li, L.-P. Ma, and H.-M. Cheng, "Advanced materials for energy storage," *Advanced Materials*, vol. 22, no. 8, pp. E28–E62, 2010.

[3] M. Jian, B. Liu, G. Zhang, R. Liu, and X. Zhang, "Adsorptive removal of arsenic from aqueous solution by zeolitic imidazolate framework-8 (ZIF-8) nanoparticles," *Colloids and Surfaces A: Physicochemical and Engineering Aspects*, vol. 465, pp. 67–76, 2015.

[4] T. A. Hamdalla, A. M. Aboraia, V. V. Shapovalov et al., "Synchrotron-based operando X-ray diffraction and X-ray absorption spectroscopy study of $LiCo_{0.5}Fe_{0.5}PO_4$ mixed d-metal olivine cathode," *Scientific Reports*, vol. 13, no. 1, Article ID 2169, 2023.

[5] L. G. Trung, M. K. Nguyen, T. D. Hang Nguyen, V. A. Tran, J. S. Gwag, and N. T. Tran, "Highly efficient degradation of reactive black KN-B dye by ultraviolet light responsive ZIF-8 photocatalysts with different morphologies," *RSC Advances*, vol. 13, no. 9, pp. 5908–5924, 2023.

[6] C.-W. Chang, Y.-H. Kao, P.-H. Shen, P.-C. Kang, and C.-Y. Wang, "Nanoconfinement of metal oxide MgO and ZnO in zeolitic imidazolate framework ZIF-8 for CO_2 adsorption and regeneration," *Journal of Hazardous Materials*, vol. 400, Article ID 122974, 2020.

[7] B. Chameh, M. Moradi, S. Hajati, and F. A. Hessari, "Design and construction of ZIF(8 and 67) supported Fe_3O_4 composite as advanced materials of high performance supercapacitor," *Physica E: Low-dimensional Systems and Nanostructures*, vol. 126, Article ID 114442, 2021.

[8] H. Li, Y. Chen, Q. Ma et al., "The effect of ZIF-8 on the phase structure and morphology of bead-like $CuMn_2O_4$/ZnO photocatalystic electrospun nanofibers," *Materials Letters*, vol. 216, pp. 199–202, 2018.

[9] Z. Lai, "Development of ZIF-8 membranes: opportunities and challenges for commercial applications," *Current Opinion in Chemical Engineering*, vol. 20, pp. 78–85, 2018.

[10] H. N. Abdelhamid, "Biointerface between ZIF-8 and biomolecules and their applications," *Biointerface Research in Applied Chemistry*, vol. 11, no. 1, pp. 8283–8297, 2021.

[11] T. A. Hamdalla, M. M. Aljohani, and A. M. Alsharari, "Synthesis and characterization of PANI/$ZnFe_2O_4$ nRs with different doping concentrations for potential applications in various fields," *Journal of Spectroscopy*, vol. 2023, Article ID 1679035, 10 pages, 2023.

[12] K. S. Park, Z. Ni, A. P. Côté et al., "Exceptional chemical and thermal stability of zeolitic imidazolate frameworks," *Proceedings of the National Academy of Sciences*, vol. 103, no. 27, pp. 10186–10191, 2006.

[13] R. Reveendran and M. A. Khadar, "Structural, optical and electrical properties of Cu doped α-Fe_2O_3 nanoparticles," *Materials Chemistry and Physics*, vol. 219, pp. 142–154, 2018.

[14] S. Kumar, A. Kumar, T. Malhotra, and S. Verma, "Characterization of structural, optical and photocatalytic properties of silver modified hematite (α-Fe_2O_3) nanocatalyst," *Journal of Alloys and Compounds*, vol. 904, Article ID 164006, 2022.

[15] M. Ahmed Alsharif, A. Alatawi, T. A. Hamdalla, S. Alfadhli, and A. A. A. Darwish, "CuO nanoparticles mixed with activated BC extracted from algae as promising material for supercapacitor," *Scientific Reports*, vol. 13, no. 1, Article ID 22321, 2023.

[16] X. Zhou, G. Wang, L. Zhang et al., "Enhanced thermoelectric properties of Ba-filled skutterudites by grain size reduction and Ag nanoparticle inclusion," *Journal of Materials Chemistry*, vol. 22, no. 7, pp. 2958–2964, 2012.

[17] H. Li, J. Wang, Q. Chu, Z. Wang, F. Zhang, and S. Wang, "Theoretical and experimental specific capacitance of polyaniline in sulfuric acid," *Journal of Power Sources*, vol. 190, no. 2, pp. 578–586, 2009.

[18] Y. Hu, Z. Liu, J. Xu, Y. Huang, and Y. Song, "Evidence of pressure enhanced CO_2 storage in ZIF-8 probed by FTIR spectroscopy," *Journal of the American Chemical Society*, vol. 135, no. 25, pp. 9287–9290, 2013.

[19] S. Sun, Z. Yang, J. Cao, Y. Wang, and W. Xiong, "Copper-doped ZIF-8 with high adsorption performance for removal of tetracycline from aqueous solution," *Journal of Solid State Chemistry*, vol. 285, Article ID 121219, 2020.

[20] S. Alfadhli, A. A. A. Darwish, S. A. Al-Ghamdi et al., "Synthesis, characterization, optical, and sensing investigations for Fe-BDC doped with 10 wt.% of activated food waste biochar," *Journal of Asian Ceramic Societies*, vol. 12, pp. 1–11, 2023.

[21] Z.-Y. Zhou, N. Tian, J.-T. Li, I. Broadwell, and S.-G. Sun, "Nanomaterials of high surface energy with exceptional properties in catalysis and energy storage," *Chemical Society Reviews*, vol. 40, no. 7, pp. 4167–4185, 2011.

[22] K. Kierzek and G. Gryglewicz, "Activated carbons and their evaluation in electric double layer capacitors," *Molecules*, vol. 25, no. 18, Article ID 4255, 2020.

[23] J. C. Wang, S. P. Hill, T. Dilbeck, O. O. Ogunsolu, T. Banerjee, and K. Hanson, "Multimolecular assemblies on high surface area metal oxides and their role in interfacial energy and electron transfer," *Chemical Society Reviews*, vol. 47, no. 1, pp. 104–148, 2018.

[24] Z. Abdi, M. Vandichel, A. S. Sologubenko et al., "The importance of identifying the true catalyst when using Randles–Sevcik equation to calculate turnover frequency," *International Journal of Hydrogen Energy*, vol. 46, no. 76, pp. 37774–37781, 2021.

[25] P. Simon and Y. Gogotsi, "Materials for electrochemical capacitors," *Nature Materials*, vol. 7, no. 11, pp. 845–854, 2008.

[26] J. Chmiola, G. Yushin, Y. Gogotsi, C. Portet, P. Simon, and P. L. Taberna, "Anomalous increase in carbon capacitance at pore sizes less than 1 nanometer," *Science*, vol. 313, no. 5794, pp. 1760–1763, 2006.